Chemical Engineering Journal 386 (2020) 123988

Contents lists available at ScienceDirect

Chemical Engineering Journal

journal homepage: www.elsevier.com/locate/cej

# Adoption of 3D printed highly conductive periodic open cellular structures as an effective solution to enhance the heat transfer performances of compact Fischer-Tropsch fixed-bed reactors

Laura Fratalocchi, Gianpiero Groppi, Carlo Giorgio Visconti, Luca Lietti, Enrico Tronconi*

*Politecnico di Milano, Dipartimento di Energia, Via La Masa, 34, 20156 Milano, Italy*

## HIGHLIGHTS

- 3D printed Periodic Open Cellular Structures (POCS) first time applied to FTS.
- Highly conductive (Al) POCS enhance heat management in packed-bed FTS reactors.
- Packed Al POCS enable 80% CO conversion with excellent T-control.
- Packed Al POCS are an intensification strategy for compact tubular reactors.
- POCS enable a good control of the geometry and optimization of the cell topology.

## GRAPHICAL ABSTRACT

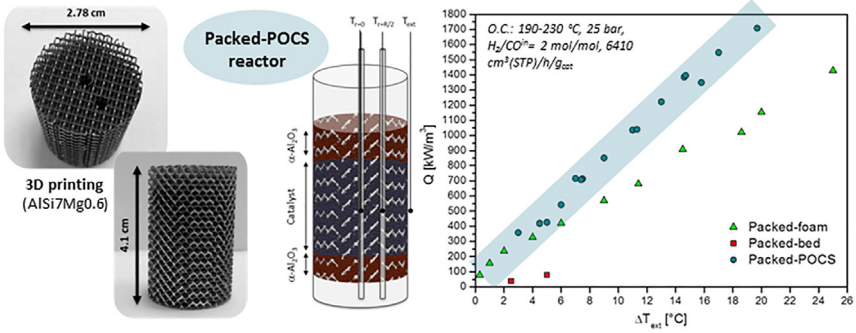


## ARTICLE INFO

*Keywords:*
Fischer-Tropsch synthesis
Conductive structured catalysts
Periodic open cellular structure
Heat transfer
Process intensification
Catalyst 3D printing

## ABSTRACT

Heat transfer is universally recognized as a key challenge for the intensification of the Fischer-Tropsch (FT) process in compact fixed-bed reactors. For the first time in the scientific literature we demonstrate experimentally that the adoption of a highly conductive periodic open cellular structure (POCS, 3D-printed in AlSi7Mg0.6 by Selective Laser Melting) packed with catalysts pellets is a promising solution to boost heat exchange in fixed-bed FT reactors. This reactor configuration enabled us to assess the performances of a highly active Co/Pt/$Al_2O_3$ catalyst packed into the POCS at process conditions relevant to industrial Fischer-Tropsch operation. Unprecedented performances (CO conversion ≈ 80%) could be thus achieved thanks to an outstanding heat management. In fact, almost flat axial and radial temperature profiles were measured along the catalytic bed even under the most severe process conditions (i.e. high CO conversions corresponding to high volumetric heat duties), demonstrating the effective potential of this reactor concept to manage the strong exothermicity of the FT reaction.

The heat transfer of the packed-POCS reactor outperformed both packed-bed and packed-foam reactors, granting smaller radial temperature gradients in the catalytic bed, as well as smaller temperature differences at the reactor wall, with larger volumetric power releases. The strengths of the packed-POCS reactor configuration are its regular geometry, which enhances the effective radial thermal conductivity, and the improved contact between the structure and the reactor wall, which governs the limiting wall heat transfer coefficient.

* Corresponding author.
*E-mail address:* enrico.tronconi@polimi.it (E. Tronconi).

https://doi.org/10.1016/j.cej.2019.123988
Received 30 August 2019; Received in revised form 21 December 2019; Accepted 28 December 2019
Available online 30 December 2019

**Nomenclature**

| | |
|---|---|
| $d_{cell}$ | cell diameter of the structure [mm] |
| $d_{pellet}$ | diameter of the catalyst pellet [μm] |
| $I.\ D.$ | internal diameter [cm] |
| $O.\ D.$ | outer diameter [mm] |
| $F_i^{out}$ | molar flow of the ith species leaving the reactor [mol/s] |
| $F_{CO}^{in}$ | is the CO molar flow fed to the reactor [mol/s] |
| $MW_i$ | molecular weight of the ith species [g/mol] |
| $n_i$ | carbon atom number of the ith species [–] |
| $Q$ | volumetric heat duty [W/m$^3$] |
| $S_i$ | selectivity to the ith species [%] |
| $S_{CO2}$ | selectivity to carbon dioxide [%] |
| $V_{cat}$ | catalyst volume [m$^3$] |
| $w_{cat}$ | catalyst weight [$g_{cat}$] |
| $X_{CO}$ | CO conversion [%] |
| $Y_{C5+}$ | specific yield of $C_{5+}$ hydrocarbons [g/h/$g_{cat}$] |
| $\varepsilon_{pocs}$ | void fraction of the POCS [–] |
| $\varepsilon_{PB}$ | packed-bed porosity [–] |
| $\Delta H_R^0$ | standard reaction enthalpy [kJ/$mol_{CO}$] |
| $\Delta T_{cat}$ | axial temperature difference [°C] |
| $\Delta T_{rad}$ | radial temperature difference [°C] |
| $\Delta T_{ext}$ | overall radial temperature difference [°C] |
| $T_{ext}$ | temperature at the outer wall of the reactor tube [°C] |
| $\alpha_{C15+}$ | chain growth probability [–] |

*Abbreviations*

| | |
|---|---|
| FTS | Fischer-Tropsch synthesis |
| LTFT | Low-temperature Fischer-Tropsch |
| POCS | periodic open cellular structure |
| SLM | selective laser melting |
| EDM | electrical discharge machining |
| BET/BJH | Brunauer, Emmet, and Teller/ Barrett, Joyner, and Halenda |
| ICP-MS | inductively coupled plasma mass spectrometry |
| XRD | X-ray diffraction |
| DOR | degree of reduction |
| T.o.S. | time on stream [h] |
| GHSV | gas hourly space velocity [$cm^3$(STP)/h/$g_{cat}$] |
| O/P | olefin to paraffin ratio |
| ASF | Anderson-Schulz-Flory |

## 1. Introduction

Since its discovery in 1923, the Fischer-Tropsch synthesis (FTS) has been recognized as a technology of great potential to convert carbon monoxide and hydrogen from large coal and natural gas reservoirs into synthetic liquid fuels and valuable chemicals. In the last decade, the interest in the FTS is even more increased in view of exploiting both associated and remote natural gas fields to produce liquid fuels.

The so called low-temperature Fischer-Tropsch (LTFT) synthesis is commonly carried out over supported cobalt-based catalysts at 20–30 bar and at temperatures below 240 °C.

The strong exothermicity of the LTFT ($\Delta H_R^0 \approx -165$ kJ/$mol_{CO}$), combined with its strong temperature sensitivity, causes temperature control issues, especially in the development of intensified compact fixed-bed reactors [1]. An efficient removal of the reaction heat at high CO conversion levels is thus crucial to reduce as much as possible the formation of hot spots within the catalyst bed [2]. The presence of strong temperature gradients negatively affects the catalyst selectivity since the LTFT product distribution is strongly dependent on the reaction temperature. A good thermal management of the reactor is also fundamental to avoid safety risks associated with thermal runaway.

Heat transfer in multitubular packed-bed reactors within each tube is governed by the fluid-phase convection, since heat transfer by thermal conduction is limited by contact point resistances between the catalyst particles and between the particles and the reactor walls [3]. Accordingly, at the industrial scale heat transfer issues force to limit the CO conversion per pass and to recycle the unconverted syngas as well as a considerable fraction of the liquid reaction products at high flow rates. For kinetically controlled reactions, like the FTS, the requirement of high flow rates imposes the use of long (i.e. $>$ 10 m) tubes, so to not affect the contact time. Indeed, a decrease of the bed contact time would result in a decreased CO conversion together with a reduced selectivity to long-chain hydrocarbons [4].

However, boosting the heat transfer by increasing the fluid velocity results in an increase of the pressure drops, too, and makes the reactor less flexible for scale down to the compact scale [5].

To date, in fact, the small-scale and modular FT technology is becoming increasingly popular in order to exploit underutilized small gas reservoirs in remote areas but also other feedstocks available in limited amounts only, such as associated gas produced during oil extraction or syngas produced from biomass. The need for short reactors (≈1–3 m long) rules out conventional multitubular packed-bed designs since heat transfer by thermal convection becomes limited by the low flow velocity associated with operation at constant space velocity [6].

Several intensified structured reactors, based on highly conductive inserts, have been proposed for the compact FTS, such as microchannels, closed cross flow structures, micro-fibrous entrapped catalysts, honeycomb monoliths, micro-monoliths and foams reactors [7–27]. Among those structures, open-cell foams are particularly attractive since they have high porosity, low density, high mechanical strength and large surface area. Also, open-cell foams can be made of highly thermally conductive metals, such as Al or Cu. Thanks to the continuous, thermally connected structure, this offers a good potential for the improvement of the heat transfer properties of a FTS packed-bed reactor [16,19–20], particularly at low gas flow rates, since the primary radial heat exchange mechanism is shifted from convection to conduction within the thermally connected solid matrix of the foam [16].

We have recently demonstrated [20] that packing the catalyst pellets into a metallic (Al) foam is an effective solution to enhance the heat transfer performances of tubular FTS reactors, while granting at the same time a high catalyst inventory and acceptable low pressure drops. Indeed, the catalyst load that can be packed in the open-cell foam is much greater than the amount that can be coated on the same foam, thus boosting the productivity per reactor volume. In addition, “packing” the foam overcomes all the problems related to the coating process, to the catalyst loading and unloading procedures, and to the replacement of the spent catalyst [20].

Another advantage of this compact technology is the fact that, thanks to the low fluid velocity, the pressure drops per unit of length are strongly reduced. This means that small catalytic pellets ($d_{pellet} \approx$ 400–800 μm [6]) can be used while granting at the same time acceptable pressure drops (see Supplementary material, Text S4).

Open-cell foams, however, suffer from some drawbacks associated with their manufacturing processes, which do not allow a fine control of the geometry: the highly irregular, somewhat random morphology of the foam, characterized by wide variations of cell size and strut diameter over the entire structure, makes the systematic investigation of both geometry and heat transfer properties rather complex. To overcome such an issue, Schwieger, Freund and coworkers [28–32] have proposed the adoption of periodic open cellular structures (POCS). POCS are characterized by periodic spatial arrangements of representative unit cells with well-defined geometries (e.g. cubes,

tetrakaidecahedra or diamonds). This results in highly ordered structures, which combine the advantages deriving from their regularity (typical of honeycomb monoliths) with the possibility of radial mixing (typical of open-cell foams) [28–32]. These structures can be fabricated by means of additive manufacturing techniques (3D printing), a manufacturing technique that is becoming increasingly popular and that enables high design flexibility, as well as the production of highly reproducible structures with an excellent control of their geometry [28–32]. Virtually any cell shape is feasible.

Furthermore, in contrast to open-cell foams, POCS are designed with a uniform strut diameter (i.e. constant cross-section along the strut axis), which allows the enhancement of the effective conductivity in radial direction up to 30% with respect to conventional open-cell foams [33].

Moreover, the high design flexibility potentially allows the optimization of the cell topology depending on the application.

Concerning their heat transfer efficiency, POCS significantly outperforms randomly packed-beds owing to the considerable contribution of the conductive heat transfer mechanism in cellular structures [32]. This aspect has been first investigated by Busse et al. [32] through numerical simulations of a non-reactive system.

Based on these premises, for the first time in the scientific literature, in this work we demonstrate experimentally at the lab scale that the heat transport performances of a FTS fixed-bed reactor can be enhanced through the adoption of a periodic open cellular structure made of aluminum. The heat transfer efficiency of the herein proposed "packed-POCS" is then compared with that obtained with the packed-foam reactor technology proposed in our recent paper [20], and with the conventional randomly packed-bed reactor.

## 2. Experimental

### 2.1. Catalyst preparation and characterization

The catalyst used in this work is a Pt-promoted Co-based catalyst containing 23 wt% of Co and 0.1 wt% of Pt, supported on γ-$Al_2O_3$ pellets (Sasol Puralox®) with an average diameter of 300 μm to limit pressure drops while minimizing pore diffusion limitations. More details on the catalyst preparation method, as well as on the chemical and physical properties of the Co/Pt/$Al_2O_3$ catalyst can be found in [34]. The most important characteristics are summarized in Table 1.

The surface area and pore volume of the calcined catalyst are determined by BET/BJH analysis. The effective catalyst composition is obtained by ICP-MS analysis and it is in good agreement with the nominal Co and Pt loadings of the catalyst. The average size of $Co_3O_4$ and metallic Co crystallites are determined by in-situ X-ray diffraction after calcination and $H_2$-reduction treatment at 400 °C for 17 h. The degree of reduction (DOR) of the catalyst is calculated from magnetic measurements after in-situ reduction [34].

### 2.2. Packed-POCS reactor

The POCS used in this study is manufactured by 3D printing (Renishaw AM250) based on the Selective Laser Melting technology and using AlSi7Mg0.6 (composition: 92.7 wt% Al, 6.8 wt% Si and 0.5 wt% Mg) as starting metal powder.

The POCS is characterized by repeated diamond cells with a diameter ($d_{cell}$) of 3 mm and a void fraction ($\varepsilon_{pocs}$) of 0.890. Due to manufacturing issues (i.e. structure stability during the printing process), the POCS is printed with an outer metallic skin 1 mm thick later removed by electrical discharge machining (EDM).

As shown in Fig. 1a, the final shape of the POCS is a cylinder with a length of 4.1 cm and a diameter of 2.78 cm. Notably, the diameter of the POCS matches the internal diameter (I.D.) of the stainless steel reactor used in the FTS activity tests, so to ensure good contact and avoid dead space ("gap") between the tube and the cellular structure. The structure is manually forced into the reactor tube by using a T-handle, sliding arm bar clamp. Once loaded the structure into the tube, no relative motion was possible, thus resulting in a weak interference. The latter becomes stronger during FTS due to the operating temperatures (190–230 °C) that cause differential thermal expansion of the two materials (AlSi7Mg0.6 versus 316L stainless-steel).

Two axial through holes of 3.2 mm diameter are located at the centerline of the structure and at 7 mm from the middle in radial position (i.e. at half of the radius of the structure) (Fig. 1a), designed for the insertion of stainless steel thermowells (1/8″ O.D.), which accommodate two sliding J-type thermocouples (0.5 mm O.D.) (Fig. 1b).

Once the POCS is loaded in the tubular reactor and the thermowells are positioned into the structure, the system is packed as schematically shown in Fig. 1b. Initially, ≈4.8 g of α-$Al_2O_3$ pellets ($d_{pellet}$ = 300 μm) are poured into the POCS, thus forming a 1.1 cm deep layer. Then, 7.2 g of Co/Pt/$Al_2O_3$ catalyst diluted with a very small amount of α-$Al_2O_3$ (catalyst:α-$Al_2O_3$ = 7.2:1 w/w) with the same particle size are poured into the POCS, thus forming a catalyst layer of 1.9 cm. Finally, 4.8 g of α-$Al_2O_3$ pellets ($d_{pellet}$ = 300 μm) are packed into the POCS so to fill the last 1.1 cm of the structure.

The resulting average catalyst volumetric density, defined as the ratio of the catalyst mass (7.2 g) to the reactor volume occupied by the catalyst bed (11.2 $cm^3$), is 0.64 g/$cm^3$.

Notably, we found that the amount of pellets loaded into the POCS well corresponds to the amounts of pellets that can be loaded in a packed-bed with the same volume of the voids (cells) of the structure and a packed-bed porosity ($\varepsilon_{PB}$) of 0.376. This clearly indicates that, due to the high $d_{cell}/d_{pellet}$ ratio, the small catalyst pellets can uniformly fill the voids of the structure and the presence of the POCS struts has negligible effects on the packing effectiveness.

### 2.3. Catalytic tests

#### 2.3.1. Packed-POCS reactor

The packed-POCS is tested in the FTS for several hours of time on stream (T.o.S. ≈ 600 h) using a fully automated lab-scale rig [35] equipped with a stainless-steel tubular reactor 2.78 cm I.D., 85 cm long inserted in a three-zone split tube furnace (Carbolite, TVS/600) (a sketch of the reactor setup is given in the Supplementary material, Text S1). More details on the reactor and on the lab-scale apparatus can be found in [35] and in references therein.

Prior to exposing the catalyst to syngas, the sample is reduced in situ in $H_2$ (Sapio, 99.995 mol.%) at 400 °C (heating rate = 2 °C/min) and atmospheric pressure for 17 h fed with a gas hourly space velocity (GHSV) of 5000 $cm^3$(STP)/h/$g_{cat}$.

Catalytic runs are carried out at relevant industrial process conditions: T = 190–230 °C (measured at the centerline mid-point of the catalyst bed), P = 25 bar, $H_2/CO^{in}$ = 2.0 mol/mol, GHSV = 6410 $cm^3$(STP)/h/$g_{cat}$, inerts ($N_2$ + Ar) in the feed = 24 vol %.

The unconverted reactants and the full spectrum of products are measured by on-line and off-line gas-chromatography. Details on the product collection and analysis procedures can be found elsewhere [35].

In order to collect representative activity data, the packed-POCS is tested for more than 70 h at each operating condition. In order to check

**Table 1**
Properties of the Co/Pt/$Al_2O_3$ catalyst [25].

| $S_{BET}$[a] [$m^2$/g] | $V_{pore}$[a] [$cm^3$/g] | $X_{Co}$[b] [wt%] | $X_{Pt}$[b] [wt%] | $d_{Co3O4}$[c] [nm] | $d_{Co}$[c] [nm] | DOR[d] [%] |
|---|---|---|---|---|---|---|
| 59 | 0.20 | 22.80 ± 0.59 | 0.110 ± 0.002 | 21 | 9 | 100 |

Calculated from [a]BET/BJH; [b]ICP-MS; [c]in-situ XRD and [d]in-situ magnetic measurements by repeating the experiments at least twice.

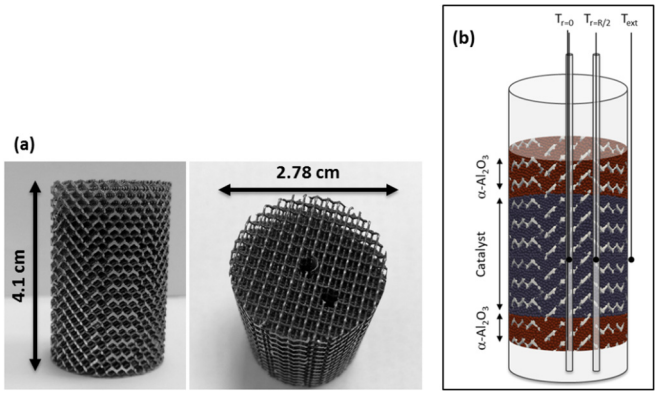


**Fig. 1.** (a) Images of the Al periodic open cellular structure (POCS) and (b) qualitative scheme of the POCS loaded into the reactor and packed with catalyst pellets and α-$Al_2O_3$. The position of the thermocouples is also shown.

the attainment of steady state conditions, multiple data at the same experimental condition are collected for more than 48 consecutive hours. Data are considered steady when the CO conversion ($X_{CO}$, Eq. (1)) and the selectivity to the main FTS products ($S_i$, Eq. (2)) varied within less than 5% in 48 h on a relative basis:

$$X_{CO}\ [\%] = \left(1 - \frac{F_{CO}^{out}}{F_{CO}^{in}}\right) \bullet 100 \tag{1}$$

$$S_i\ [\%] = \frac{F_i^{out} \bullet n_i}{\sum_i^{NP} (F_i^{out} \bullet n_i) + F_{CO2}^{out}} \bullet 100 \tag{2}$$

In Eqs (1) and (2), $F_i^{out}$ is the molar flow of the ith species leaving the reactor, $F_{CO}^{in}$ is the CO molar flow fed to the reactor, $n_i$ is the carbon atom number of the ith species and NP (=49) is the number of carbon atoms in the heaviest hydrocarbon identified at the product pool. The selectivity to carbon dioxide is calculated as in Eq. (3):

$$S_{CO2}\ [\%] = \frac{F_{CO2}^{out}}{F_{CO}^{in} - F_{CO}^{out}} \bullet 100 \tag{3}$$

The specific yield of $C_{5+}$ hydrocarbons ($Y_{C5+}$) is calculated as in Eq. (4), where $MW_i$ is the molecular weight of the ith species and $w_{cat}$ the catalyst weight:

$$Y_{C5+}\ [g/h/g_{cat}] = \frac{\sum_{i\geq 5}^{NP} (F_i^{out} MW_i)}{w_{cat}} \tag{4}$$

The catalyst stability is verified by comparing the catalyst performances (measured at 190 °C, 25 bar, $H_2/CO^{in}$ = 2 mol/mol, GHSV = 6410 $cm^3$(STP)/h/$g_{cat}$, inerts ($N_2$ + Ar) in the feed = 24 vol %) at the beginning (T.o.S. ≈ 70 h) and at the end (T.o.S. ≈ 586 h) of the experimental test.

Carbon balances, calculated as moles of C contained in the reaction products divided by the moles of CO converted, always close within ± 10%, being typically within ± 5%.

The volumetric heat duty (Q) is calculated according to Eq. (5):

$$Q\ [W/m^3] = \frac{-\Delta H_R^0 \bullet F_{CO}^{in} \bullet X_{CO}}{V_{cat}} \tag{5}$$

where $\Delta H_R^0$ is the standard reaction enthalpy calculated on the basis of the products distribution obtained at different temperatures (see Supplementary material, Text S2) and $V_{cat}$ is the volume occupied by the catalyst in the reactor.

#### 2.3.2. Kinetic measurements

As already reported in [20], loading the same tubular reactor (2.78 cm I.D.) with 7.2 g of catalyst particles only, i.e. without the addition of a conductive internal, lead to the thermal runaway of the reactor already at the very low catalyst temperature of 195 °C, even if the catalyst was diluted with a large amount of inert α-$Al_2O_3$ (catalyst: α-$Al_2O_3$ = 1:1.7 w/w). This clearly reflects the impossibility to perform a proper kinetic investigation at these experimental conditions.

Therefore, in this work the kinetic measurements in the absence of conductive internals are carried out in the same lab-scale rig used to test the structured catalyst but with a different tubular reactor with smaller internal diameter (1.1 cm I.D.). The same batch of Co/Pt/$Al_2O_3$ catalyst used in the packed-POCS experimental runs is loaded in the reactor but in a lower amount (≈2 $g_{cat}$) and diluted with a larger amount of α-$Al_2O_3$ pellets (catalyst/α-$Al_2O_3$ = 1:4 v/v) with the same particle size of the catalyst ($d_{pellet}$ = 300 μm), to prevent local hot-spots (length of diluted catalytic bed = 13 cm).

The catalyst temperature is set at the midpoint of the catalyst bed in axial direction through a 0.5 mm thick J-type thermocouple located into an axial thermowell (2 mm O.D.).

The set-up is the same adopted in previous kinetic studies [36–38] except for the particles size ($d_{pellet}$ = 75–100 μm in [36–38]). The absence of intra-particle and inter-particle concentration and temperature gradients has been checked by literature criteria [39–41]. The results are reported in the Supplementary material, Text S3.

### 2.4. Thermal behaviour of the packed-POCS reactor

Axial temperature profiles along the catalyst bed are measured at different radial positions by sliding thermocouples (0.5 mm O.D.) inserted into the thermowells located at the centreline and at the half radius position of the catalyst bed, respectively (Fig. 1b).

The axial temperature difference ($\Delta T_{cat}$) is defined as the difference between the maximum and the minimum temperature recorded along the catalyst bed at the centerline. The internal radial temperature difference ($\Delta T_{rad}$) is defined as the difference between the temperature reading at the mid-point of the catalyst bed in axial (r = 0) and half radius (r = R/2) position.

Another stainless steel thermowell (1/8″ O.D.), protecting a fixed J-type thermocouple (0.5 mm O.D.), is located at the outer wall of the reactor tube ($T_{ext}$), in correspondence to the middle of the catalyst bed (Fig. 1b). This enables to evaluate the overall radial temperature difference ($\Delta T_{ext}$), defined as the difference between $T_{ext}$ and the temperature reading at the center of the catalyst bed.

Prior to the reactivity runs, a blank test is carried out at different temperatures in the range of 190–230 °C and keeping constant the other operative conditions (25 bar, $H_2/CO^{in}$ = 2 mol/mol, GHSV = 6410 $cm^3$(STP)/h/$g_{cat}$, inerts ($N_2$ + Ar) in the feed = 24 vol %), so to identify the isothermal zone of the tubular reactor in which the catalyst should be located. For this purpose, the reactor is loaded with inert α-$Al_2O_3$ pellets and axial temperature profiles are measured along the reactor. A temperature difference less than 0.5 °C is obtained along 10 cm of the tube. Furthermore, both $\Delta T_{rad}$ and $\Delta T_{ext}$ are found to be negligible.

## 3. Results and discussion

### 3.1. Packed-POCS reactor

The performances of the packed-POCS reactor are shown in terms of CO conversion versus T.oS. (Fig. 2) and selectivity to the main FTS products (Figs. 3–7) at different temperatures. The data obtained with the conventional kinetic tests at the same temperatures are also shown for comparison purposes.

Fig. 2 shows that a CO conversion of around 20% is measured already at 190 °C, a temperature lower than that commonly used for the FTS (210–230 °C). This clearly indicates the high activity of the adopted Pt-promoted catalyst [34].

Upon increasing the temperature, a wide range of CO conversions is obtained over the packed-POCS reactor up to 80% at 230 °C (Fig. 2).

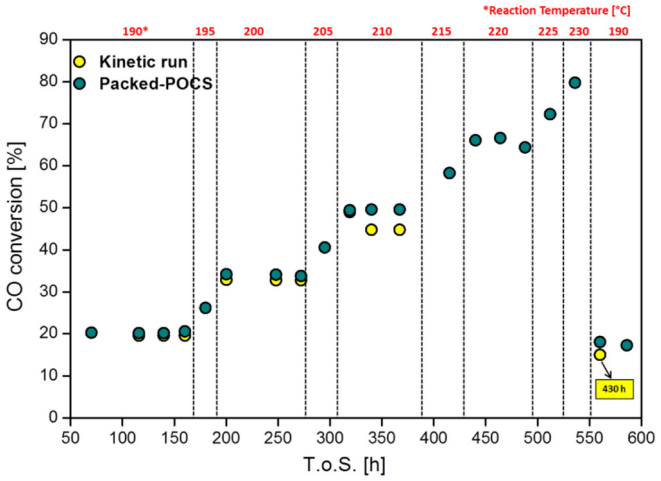


**Fig. 2.** Evolution of the CO conversion with time on stream (T.o.S.) measured in the packed-POCS reactor (green circles) and during the kinetic experiment (yellow circles) at different temperatures. P = 25 bar, $H_2/CO^{in}$ = 2 mol/mol, GHSV = 6410 $cm^3$(STP)/h/$g_{cat}$, inerts = 24 vol%. (For interpretation of the references to colour in this figure legend, the reader is referred to the web version of this article.)

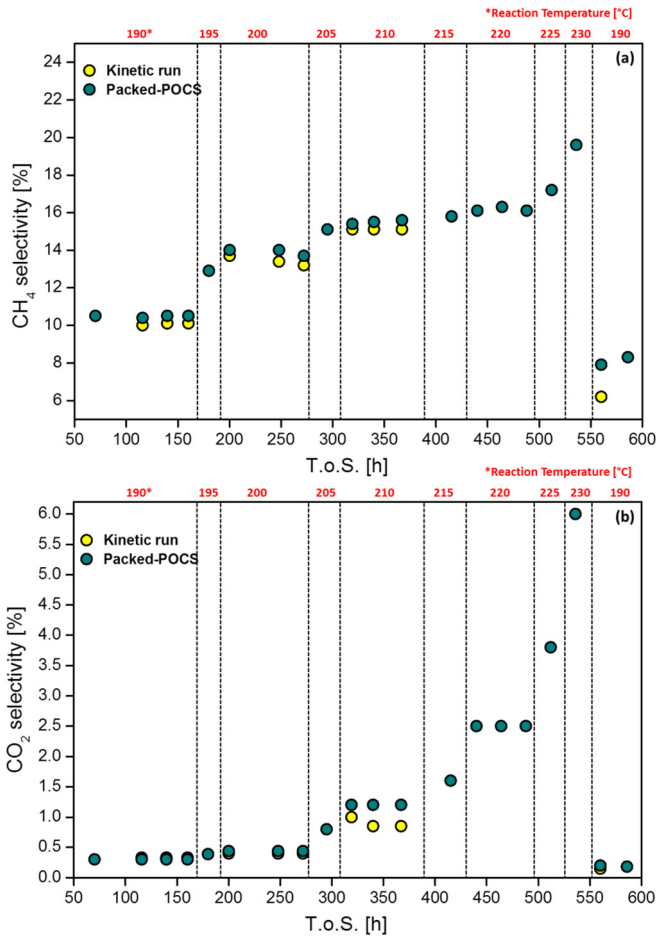


**Fig. 3.** Evolution of the selectivity to (a) $CH_4$ and (b) $CO_2$ with time on stream (T.o.S.) measured over the packed-POCS reactor (green circle) and during the kinetic experiment (yellow circle) at different temperatures. P = 25 bar, $H_2/CO^{in}$ = 2 mol/mol, GHSV = 6410 $cm^3$(STP)/h/$g_{cat}$, inerts = 24 vol%. (For interpretation of the references to colour in this figure legend, the reader is referred to the web version of this article.)

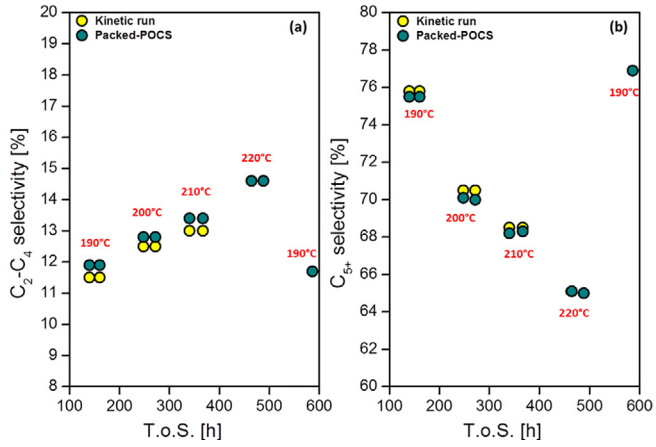


**Fig. 4.** Evolution of the selectivity to (a) $C_2$-$C_4$ and (b) $C_{5+}$ with time on stream (T.o.S.) measured over the packed-POCS reactor (green circles) and during kinetic tests (yellow circles) at different temperatures. P = 25 bar, $H_2/CO^{in}$ = 2 mol/mol, GHSV = 6410 $cm^3$(STP)/h/$g_{cat}$, inerts = 24 vol%. (For interpretation of the references to colour in this figure legend, the reader is referred to the web version of this article.)

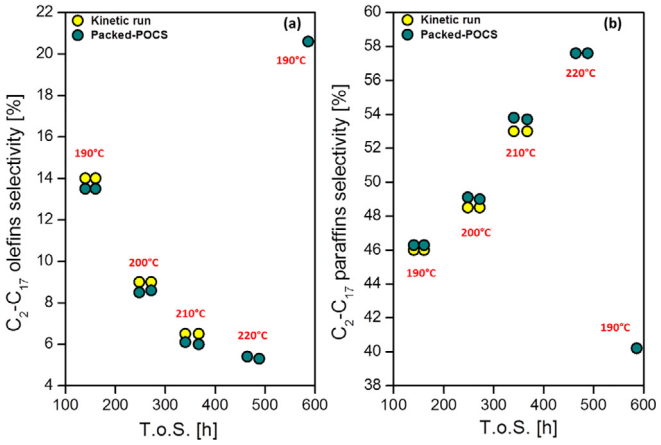


**Fig. 5.** Evolution of the selectivity to (a) olefins and (b) paraffins in the $C_2$-$C_{17}$ range with time on stream (T.o.S.) measured over the packed-POCS reactor (green circles) and during the kinetic experiment (yellow circles) at different temperatures. P = 25 bar, $H_2/CO^{in}$ = 2 mol/mol, GHSV = 6410 $cm^3$(STP)/h/$g_{cat}$, inerts = 24 vol%. (For interpretation of the references to colour in this figure legend, the reader is referred to the web version of this article.)

Noteworthy, such a high conversion value, which matches once through process requirements (i.e. the single pass CO conversion in micro-channel FT reactors developed by Velocys is usually kept between 70 and 75% [42]), is achieved without experiencing any particular problem from the temperature control side.

The selectivity to $CH_4$ measured at 190 °C is around 10.8% (Fig. 3). As expected, higher temperatures also promote the formation of $CH_4$ (Fig. 3), which caused the increase of the heat released per mole of converted CO.

The selectivity to $CO_2$ (Fig. 3), which is negligible at low temperatures, also grows on increasing temperature, in line with the increase of the water gas shift activity of the catalyst at high CO conversion levels and hence at high-water concentrations. Indeed, water is the most abundant FTS product, as the oxygen atoms of CO are mainly converted to $H_2O$.

In line with the increase of $CH_4$ selectivity, higher temperatures boost the formation of short chain hydrocarbons, as shown in Fig. 4a by $C_2$-$C_4$ species, and a corresponding decrease of the $C_{5+}$ selectivity (Fig. 4b). This increased activity towards the chain termination

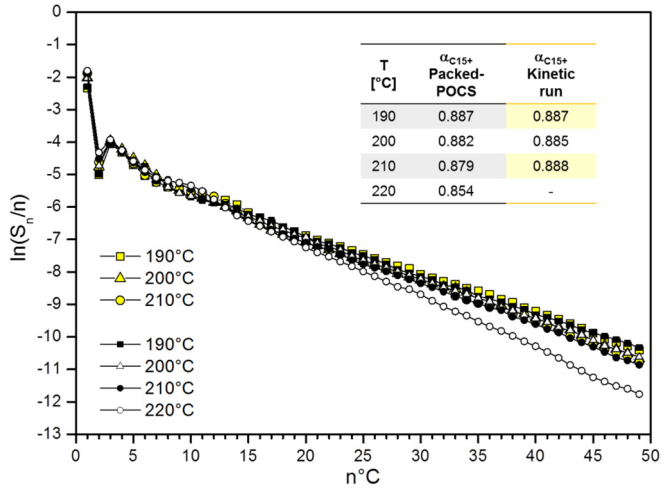


| T [°C] | $\alpha_{C15+}$ Packed-POCS | $\alpha_{C15+}$ Kinetic run |
|---|---|---|
| 190 | 0.887 | 0.887 |
| 200 | 0.882 | 0.885 |
| 210 | 0.879 | 0.888 |
| 220 | 0.854 | - |

**Fig. 6.** Hydrocarbons ASF plots as a function of the carbon number (n°C) and $\alpha_{C15+}$ values calculated for the packed-POCS reactor (black) and during the kinetic experiment (yellow) at different temperatures. P = 25 bar, $H_2/CO^{in}$ = 2 mol/mol, GHSV = 6410 $cm^3(STP)/h/g_{cat}$, inerts = 24 vol%. (For interpretation of the references to colour in this figure legend, the reader is referred to the web version of this article.)

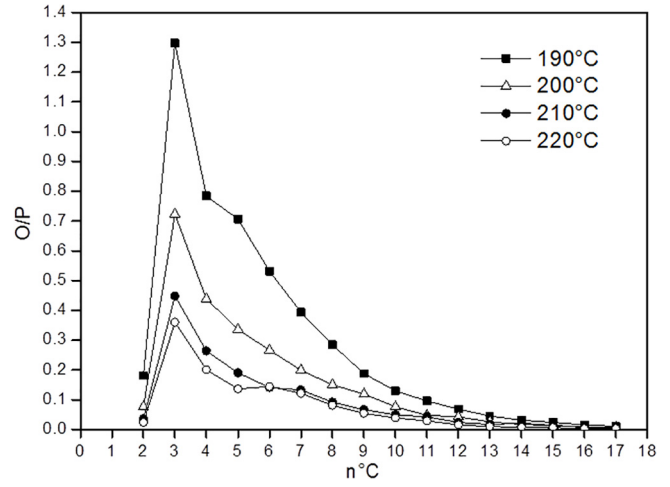


**Fig. 7.** Olefin to paraffin ratio plots in the $C_2$-$C_{17}$ range as a function of the carbon number (n°C) calculated at 190 °C (T.o.S. = 161 h), 200 °C (T.o.S. = 272 h), 210 °C (T.o.S. = 367 h) and 220 °C (T.o.S. = 488 h). P = 25 bar, $H_2/CO^{in}$ = 2 mol/mol, GHSV = 6410 $cm^3(STP)/h/g_{cat}$, inerts = 24 vol%.

reactions is accompanied by an increase of olefins hydrogenation to paraffins (Fig. 5)).

These results are confirmed by data in Fig. 6, showing the Anderson–Schulz–Flory plot calculated at different temperatures, and in Fig. 7, showing the olefin to paraffin ratio (O/P) as a function of the carbon number.

The ASF distributions exhibit the typical positive and negative deviations for methane and $C_2$ hydrocarbons, respectively, and a change of slope at a carbon number around 8. The chain growth probability ($\alpha_{C15+}$), which is calculated from the slope of the plot of $ln(S_n/n)$ against $n$ (Fig. 6) by considering the hydrocarbons with more than 15 carbon atoms [43], follows the same trend of the $C_{5+}$ selectivity. In particular, $\alpha_{C15+}$ is 0.887 at 190 °C and drops to 0.854 at 220 °C (Fig. 6).

The olefin to paraffin ratio reported in Fig. 7, which shows the well-known decreasing distribution for n > 2 with ethylene out of trend, also decreases with the increase of the reaction temperature.

Overall, these results point out that high temperatures result in

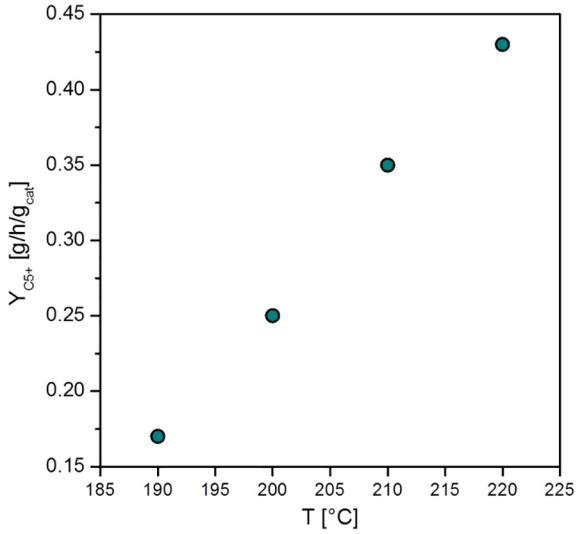


**Fig. 8.** Productivity of $C_{5+}$ hydrocarbons as a function of the reaction temperature. P = 25 bar, $H_2/CO^{in}$ = 2 mol/mol, GHSV = 6410 $cm^3(STP)/h/g_{cat}$, inerts = 24 vol%.

higher conversion rate, which is positive for the process, but cause a shift towards undesired short-chain saturated hydrocarbons. This can be explained considering that the hydrogenation rate is enhanced by increasing temperatures, thus favouring the termination step rather than the growth step in the FTS chain growth mechanism [2]. Accordingly further improvements in selectivity, which is certainly a relevant target for process optimization, could be pursued through the development of enhanced catalyst formulations [42]. The $C_{5+}$ hydrocarbons yield, plotted in Fig. 8 against the reaction temperature, increases upon increasing the temperature, indicating that the positive effect of the reaction temperature on the conversion rate prevails on the observed negative effect on the products selectivity. However, the selectivity loss with increasing temperature remains a kinetic penalty to be paid to the quest for high CO conversions suitable for once-through FTS processes.

Comparison with data collected during conventional kinetic tests performed with a highly diluted packed bed configuration shows that CO conversion is practically the same as that obtained with the packed POCS at 190 and 200 °C (Fig. 2), whereas it is slightly lower in kinetic tests at 210 °C.

Also, selectivities to the different products (Figs. 3–5) are quite similar in kinetic and packed POCS tests, proving that the insertion of the conductive structure has no negative effects on the catalytic performances.

On the other hand the maximum CO conversion reached during the kinetic experiment is 49% at 210 °C (Fig. 2). This is in line with most of the kinetic studies carried out over Co-based FT catalysts [39–41], which limit the CO conversion up to a maximum value of ≈40% in order to avoid all the issues related to the temperature control, such as the presence of hot-spots along the catalyst bed and the catalyst deactivation. Noteworthy, once reached 210 °C, the catalyst starts to slightly deactivate with time on stream, going from an initial CO conversion value of 49% down to 44% after 50 h. The deactivation of the catayst is then confirmed measuring the CO conversion at 190 °C at the end of the run (430 h), which is significantly lower (15%) than that measured after 90 h on stream (20%) at the same process conditions, and represents a more pronounced decay than observed in packed POCS tests, despite the kinetic run being significantly shorter (T.o.S. ≈ 430 h) than that carried out over the structured reactor (T.o.S. ≈ 600 h). In fact in packed POCS tests the CO conversion measured after 586 h on stream (17.5%) is only slightly below that measured after 70 h on stream (20%) at the same process conditions, with consistent modifications of

the products distribution associated with a slight decrease of the hydrogenation rate.

This is a clear indication of the fact that the adoption of a highly conductive internal enables to operate under more severe operating conditions, thus extending the feasible range of the kinetic investigations.

Fig. 9 shows the axial temperature profiles ($\Delta T_{cat}$) measured on the packed-POCS at different temperatures (190–230 °C). Limited T-differences along the catalyst bed are observed at all the investigated temperatures. Below 200 °C $\Delta T_{cat}$ is negligible, remaining small ($\Delta T_{cat}$ = 3 °C) also at 210 °C where 50% CO conversion is achieved. Then, it gradually increases with temperature up to$\Delta T_{cat}$ = 7 °C at the most severe investigated condition; i.e. 80% CO conversion. As a matter of fact, the presence of an appreciable hot-spot is detectable only at the highest investigated temperatures (Fig. 9), due to the larger heat released by the reaction.

A detailed investigation of the different contributions to the overall heat transfer performances of the system is not allowed due to the limits of our experimental set up (i.e. use of a furnace instead of a jacketed single-tube reactor). However, a preliminary analysis can be obtained by plotting the temperature driving forces, namely $\Delta T_{rad}$ (i.e. difference between the temperature reading at the mid-point of the catalyst bed in axial ($T_{r=0}$) and half radius ($T_{r=R/2}$) position) and $\Delta T_{ext}$ (i.e. difference between $T_{r=0}$ and at the outer wall of the reactor tube ($T_{ext}$)) against the volumetric heat duty Q, calculated by eq (5). The results are shown in Fig. 10.

It is worth noting that a value of 1730 kW/m$^3$, corresponding to 80% CO conversion, is reached at T = 230 °C while keeping a good temperature control of the reactor. To our knowledge, such a high value has never been previously reported in the literature for lab scale FT reactors [1].

As shown in Fig. 10, $\Delta T_{rad}$values lower than 1 °C are obtained at all the temperatures investigated. Notably, the $\Delta T_{rad}$ increases linearly with Q, going from 0.1 °C up to 0.8 °C when the reaction temperature is increased from 190 to 230 °C. This highlights the very high effective internal thermal conductivity of the ordered structure studied in this work.

Also the external temperature difference ($\Delta T_{ext}$) increases almost linearly with the increase of the volumetric heat duty (Fig. 10), in line with the exothermicity of the reaction. Such a linear trend proves that: i) the oven is acting as a heat sink and not as a heat source, since the heating elements are set to temperatures well below $T_{r=0}$ and $T_{ext}$; ii) ill-defined heat exchange conditions from the external skin of the reactor tube to the oven do not result in major anomalies affecting heat transfer within the reactor (including the likely limiting contribution of the heat resistance close to the internal reactor wall), which is the focus of the present investigation.

The fact that the $\Delta T_{ext}$ widely exceeds $\Delta T_{rad}$, increasing from 3 to 20 °C in the investigated range, indicates that most of the heat transfer resistance is confined in the near-wall region of the bed.

Noteworthy, at the end of the run, the POCS structure is easily unloaded from the reactor tube after $N_2$-treatment (1410 cm$^3$(STP)/h/$g_{cat}$) at 200 °C and atmospheric pressure for 190 h. No mechanical damages were observed. Also, the packed catalyst is easily removed from the POCS (Fig. 11). This is extremely relevant in view of the scale-up of such a technology, since it indicates that the same internal can be further used for additional catalytic runs and that the spent catalysts packed inside the cells can be conveniently replaced.

### 3.2. Comparison of the thermal behavior of Packed-POCS, Packed-foam and Packed-bed

Figs. 12 and 13 compare the thermal behavior of the packed-foam, packed-bed and packed-POCS reactor configurations by plotting the volumetric heat duty measured at different reaction temperatures against the radial and the external temperature differences, respectively. The slope of the data in Fig. 13 therefore reflects the internal heat conductivity, whereas the slope of the data in Fig. 14 is representative of an overall heat transfer coefficient including also the wall heat transfer resistance. The data related to the packed-foam and packed-bed reactors configurations are extensively discussed in [20].

The radial temperature differences measured in the packed-bed reactor (Fig. 12) are much more severe than in the packed-foam reactor, as already reported [20], and in the packed-POCS reactor. This confirms that in both the structured reactors the internal heat transfer is strongly enhanced thanks to the conductive thermally connected solid matrices of foam and POCS.

Focusing on the comparison of the two structured systems, the steeper slope of $\Delta T_{rad}$ vs Q in Fig. 12 (~ +44%) indicates that the effective thermal conductivity of the packed-POCS is significantly higher than in the packed-foam. This is partially due to the higher relative density of the POCS with respect to the foam (0.11 vs 0.092), however such a difference (+20%) is not enough to fully justify the observed improvement.

The T-differences, in fact, are likely related also to the different geometries of open foams and POCS. Bracconi et al. [33] studied by numerical simulations the influence of the geometrical properties of an open-cell foam (i.e. cell size, porosity and ratio between the node and strut diameter) on its heat conduction performances. They showed that the ratio of the node to strut diameter of the foam has a strong impact on its effective thermal conductivity at fixed porosity: high ratios penalize the heat transfer due to the reduced strut cross-sectional area. In this regard, the authors stated that an advanced design with a node-to-strut diameter ratio close to one, as adopted in the POCS of this work, can enhance the effective heat conductivity up to +30% compared to conventional open-cell foams [33]. The combination of a higher density (+20%) and of a uniform strut diameter (up to +30%) could therefore explain quantitatively the observed improvement (+40%) of the internal heat conductivity of POCS over foam.

A similar discussion applies to Fig. 13, where the volumetric heat duty calculated at different reaction temperatures is plotted against the overall radial temperature difference ($\Delta T_{ext}$). We see that the packed-POCS outperforms the packed foam reactor also in terms of overall heat transfer performances, the slope of the $\Delta T_{ext}$ vs Q packed-POCS data being about 37% steeper than for the packed foam. Notably, such a difference cannot be explained by the higher effective conductivity of the packed-POCS. In fact, in both the structured reactors $\Delta T_{ext} \gg \Delta T_{rad}$: this implies that the internal conductive heat transfer resistance

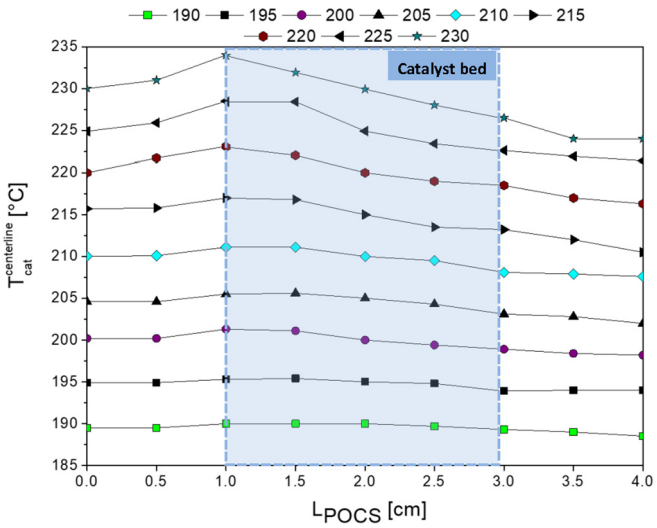


**Fig. 9.** Axial temperature profiles measured at different temperatures (T-range of 190–230 °C) in the packed-POCS reactor. The catalyst bed length is highlighted.

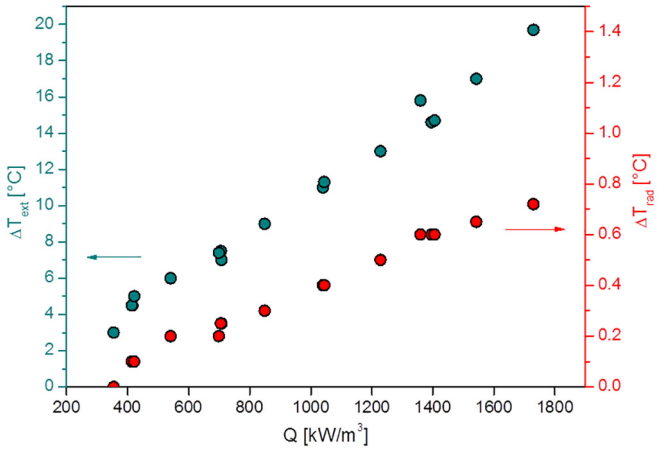


**Fig. 10.** External ($\Delta T_{ext}$) and internal ($\Delta T_{rad}$) temperature differences as a function of the volumetric heat duty measured during FTS experiment.

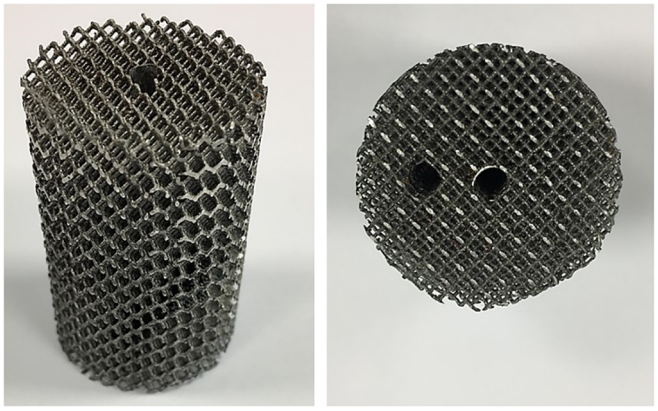

**Fig. 11.** Image of the periodic open cellular structure (POCS) unloaded from the reactor after the catalytic run and $N_2$-treatment at 200 °C for 190 h.

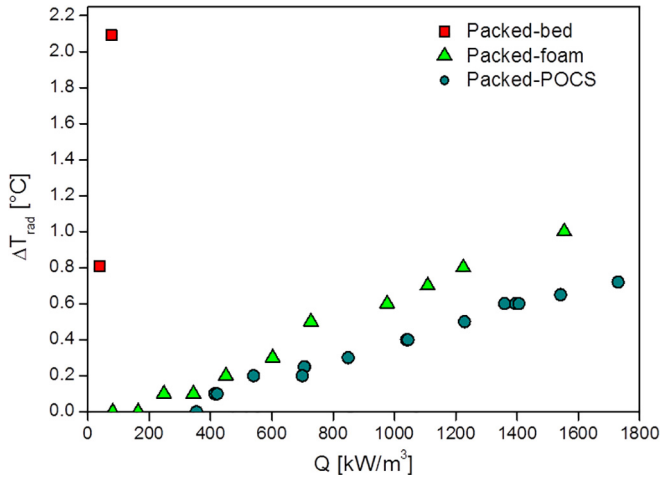


**Fig. 12.** Radial ($\Delta T_{rad}$) temperature difference as a function of the volumetric heat duty measured during FTS experiments in the packed-foam (green triangle), packed-bed (red square) and packed-POCS (blue circle) reactors. (For interpretation of the references to colour in this figure legend, the reader is referred to the web version of this article.)

provides only a minor contribution to the overall heat transfer resistance, which is dominated by the wall heat transfer resistance.

Focusing accordingly on the near-wall region, the better overall heat transfer performances of packed-POCS are possibly explained assuming

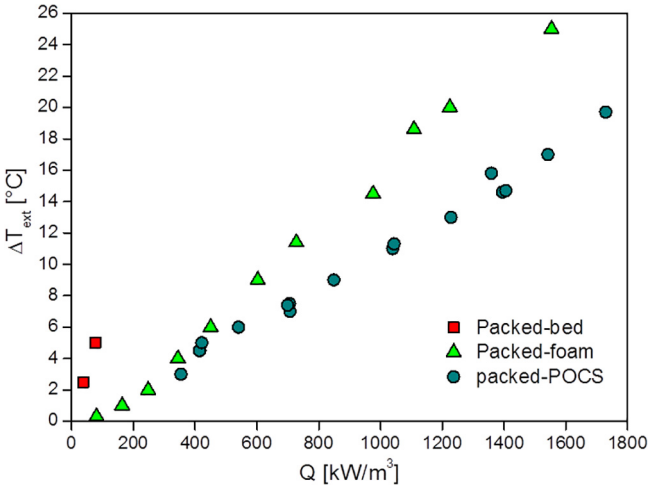


**Fig. 13.** External ($\Delta T_{ext}$) temperature difference as a function of the volumetric heat duty measured during FTS experiments carried out in the packed-foam (green triangle), packed-bed (red square) and packed-POCS (blue circle) reactors. (For interpretation of the references to colour in this figure legend, the reader is referred to the web version of this article.)

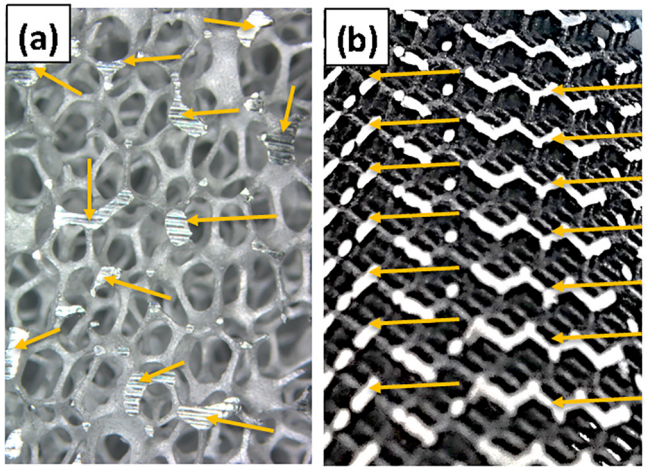


**Fig. 14.** Images of the cross-section of the (a) open-cell foam and (b) periodic open cellular structure. The yellow arrows qualitatively identify the contact points at the wall/structure interface. (For interpretation of the references to colour in this figure legend, the reader is referred to the web version of this article.)

a better contact between the reactor wall and the ordered cellular structure, which governs the wall heat transfer coefficient [44,45]. This is suggested by inspection of the images in Fig. 14, which show the presence of more regular surface available for contact in the outer border of the POCS sample, thus potentially improving the interaction between the internal structure and the reactor wall (Fig. 14b).

In order to gain insight on this aspect further investigations on the role of POCS geometrical parameters such as cell type and size and porosity are needed. Besides the use of POCS printed with an outer skin looks promising as a way to improve the structure-tube wall contact [46].

## 4. Conclusions

The intensification of the heat transfer performances of Fischer-Tropsch fixed-bed reactors is gaining considerable attention. This is due to the necessity of exploiting both associated and remote natural gas fields, as well as biomass, to produce liquid fuels, which requires scaling down the conventional packed-bed multitubular reactors to

modular compact-units, for which heat management is critical.

In our recent paper [20] we showed the possibility to overcome heat transfer limitations by adopting the conductive packed-foam reactor technology. In this work we have revealed that additional benefits can be obtained by adopting internals based on innovative conductive cellular structures with an engineered flexible design.

In particular, we have shown for the first time that heat exchange in FTS fixed-bed reactors can be further enhanced thanks to the adoption of highly conductive internals based on periodic open cellular structures. These can be fabricated by different additive manufacturing techniques, which enable the production of highly reproducible regular structures and offer more degrees of freedom in the design (e.g. cell topology optimization).

Our data clearly indicate that the adoption of a conductive packed-POCS enables to operate the FTS reactor in isothermal conditions even under very severe conditions (i.e. high CO conversions corresponding to high volumetric heat duties). As a matter of fact, nearly flat axial and radial temperature profiles within the catalyst bed were measured at all the temperatures investigated. In our tests the packed-POCS reached extreme operative conditions (80% CO conversion) that could not be accessed using the conventional randomly packed fixed-bed reactor, even if operated under milder conditions (i.e. with a catalyst volumetric density halved with respect to the POCS).

A crucial comparative experiment with the packed-foam reactor technology has pointed out that the packed-POCS shows better heat transfer performances. The strengths of the packed-POCS reactor configuration with respect to the packed-foam are the regular geometry of the POCS structure (ratio of the node to strut diameter equal to 1), which intensifies the internal thermal conductivity, and the improved contact of the ordered structure with the reactor wall, which governs the wall heat transfer coefficient.

In more general terms, with this work we confirm that packing the conductive structured reactor internal with catalyst pellets, regardless of the geometry of the structure, represents an effective solution to increase the catalyst inventory in compact structured tubular reactors. Indeed, the catalyst load which can be packed in whatever cellular structure is used (open-cell foam or POCS) is much greater than the amount which can be loaded by washcoating the same structure. In this way, the productivity per reactor volume is greatly boosted.

Noteworthy, we have shown herein also that the adoption of conductive cellular structures packed with catalyst particles enables to extend the feasible range of kinetic investigations for lab-scale studies of strongly exo- (and possibly endo-) thermic catalytic reactions.

The goal of our future research efforts is the scale up of the packed-POCS reactor technology through the assessment of its catalytic performances in the FTS under more representative conditions, i.e. in an externally cooled single-tube pilot reactor with dimensions suitable to mimic the operation of technical multitubular reactors, currently under construction.

## Acknowledgment

This project has received funding from the European Research Council under Grant Agreement no. 694910 (INTENT).

## Appendix A. Supplementary data

Supplementary data to this article can be found online at https://doi.org/10.1016/j.cej.2019.123988.

## References

[1] A. Egaña, O. Sanz, D. Merino, X. Moriones, M. Montes, Ind. Eng. Chem. Res. 57 (2018) 10187–10197.
[2] Y. Liu, D. Edouard, L.D. Nguyen, D. Begin, P. Nguyen, C. Pham, C. Pham-Huu, Chem. Eng. J. 222 (2013) 265–273.
[3] S.T. Sie, M.M.G. Senden, H.M.H. Van Wechem, Catal. Today 8 (1991) 371–394.
[4] E. Iglesia, S.C. Reyes, R.J. Madon, S.L. Soled, Adv. Catal. 39 (1993) 221–302.
[5] C.G. Visconti, E. Tronconi, L. Lietti, G. Groppi, P. Forzatti, C. Cristiani, R. Zennaro, S. Rossini, Appl. Catal. A 370 (2009) 93–101.
[6] S. Saeidi, M.K. Nikoo, A. Mirvakili, S. Bahrani, N.A.S. Amin, M.R. Rahimpour, Rev. Chem. Eng. 31 (2015) 209–238.
[7] D. Merino, O. Sanz, M. Montes, Chem. Eng. J. 327 (2017) 1033–1042.
[8] L.C. Almeida, F.J. Echave, O. Sanz, M.A. Centeno, G. Arzamendi, L.M. Gandìa, E.F. Sousa-Aguiar, J.A. Odriozola, M. Montes, Chem. Eng. J. 167 (2011) 536–544.
[9] R. Philippe, M. Lacroix, L. Dreibine, C. Pham-Huu, D. Edouard, S. Savin, F. Luck, D. Schweich, Catal. Today 147S (2009) S305–S312.
[10] M. Lacroix, L. Dreibine, B. de Tymowski, F. Vigneron, D. Edouard, D. Begin, P. Nguyen, C. Pham, S. Savin, F. Luck, M.J. Ledoux, C. Pham-Huu, Appl. Catal. A 397 (2011) 62–72.
[11] M. Sheng, H. Yang, D.R. Cahela, W.R. Yantz Jr., C.F. Gonzales, B.J. Tatarchuck, Appl. Catal. A 445–446 (2012) 143–152.
[12] M. Sheng, H. Yang, D.R. Cahela, B.J. Tatarchuck, J. Catal. 281 (2011) 254–262.
[13] N. Hooshyar, D. Vervloet, F. Kapteijn, P.J. Hamersma, R.F. Mudde, J.R. van Ommen, Chem. Eng. J. 207–208 (2012) 865–870.
[14] B. Kaskes, D. Vervloet, F. Kapteijn, J.R. van Ommen, Chem. Eng. J. 283 (2016) 1465–1483.
[15] M. Loewert, J. Hoffmann, P. Piermartini, M. Selinsek, R. Dittmeyer, P. Pfeifer, Chem. Eng. Technol. 42 (2019) 1–14.
[16] E. Tronconi, G. Groppi, C.G. Visconti, Curr. Opin. Chem. Eng. 5 (2014) 55–67.
[17] R.J. Kee, C. Karakaya, H. Zhu, Proc. Combust. Inst. 36 (2017) 51–76.
[18] L.C. Almeida, O. Sanz, D. Merino, G. Arzamendi, L.M. Gandìa, M. Montes, Catal. Today 215 (2013) 103–111.
[19] G. Groppi. E. Tronconi, C. G. Visconti, A. Tasso, R. Zennaro, Pat. WO/2015/033266.
[20] L. Fratalocchi, C.G. Visconti, G. Groppi, L. Lietti, E. Tronconi, Chem. Eng. J. 349 (2018) 829–837.
[21] R. Mystrad, S. Eri, P. Pfeifer, E. Rytter, A. Holmen, Catal. Today 147S (2009) S301–S304.
[22] I. Graf, A.K. Ruhl, B. Kraushaar-Czarnetzki, Chem. Eng. J. 244 (2014) 234–242.
[23] G. Arzamendi, P.M. Diéguez, M. Montes, J.A. Odriozola, E. Falabella Sousa-Aguiar, L.M. Gandía, Chem. Eng. J. 160 (2010) 915–922.
[24] K.S. Kshetrimayum, P. Seongho, J. Ikhwan, N. Jonggeol, H. Chonghun, Comput. Aided Chem. Eng. 37 (2015) 1355–1360.
[25] J.C. Park, N.S. Roh, D.H. Chun, H. Jung, J.-I.I. Yang, Fuel Process. Technol. 119 (2014) 60–66.
[26] H.J. Venvik, J. Yang, Catal. Today 285 (2017) 135–146.
[27] H. Becker, R. Güttel, T. Turek, Catal. Sci. Technol. 9 (2019) 2180–2195.
[28] M. Klumpp, A. Inayat, J. Schwerdtfeger, C. Körner, R.F. Singer, H. Freund, W. Schwieger, Chem. Eng. J. 242 (2014) 364–378.
[29] M. Lammermann, W. Schwieger, H. Freund, Catal. Today 273 (2016) 161–171.
[30] H. Freund, A. Inayat, M. Klumpp, T. Heidig, E. Bianchi, W. Schwieger, Chem. Ing. Technol. 88 (2016) 1209.
[31] M. Lammermann, G. Horak, W. Schwieger, H. Freund, Chem. Eng. Process. 126 (2018) 178–189.
[32] C. Busse, H. Freund, W. Schwieger, Chem. Eng. Process. 124 (2018) 199–214.
[33] M. Bracconi, M. Ambrosetti, M. Maestri, G. Groppi, E. Tronconi, Chem. Eng. Process. 129 (2018) 181–189.
[34] L. Fratalocchi, L. Lietti, C.G. Visconti, N. Fischer, M. Claeys, Catal. Sci. Technol. 9 (2019) 3177–3192.
[35] C.G. Visconti, L. Lietti, P. Forzatti, R. Zennaro, Appl. Catal. A 330 (2007) 49–56.
[36] C.G. Visconti, E. Tronconi, L. Lietti, P. Forzatti, S. Rossini, R. Zennaro, Top. Catal. 54 (2011) 786–800.
[37] C.G. Visconti, E. Tronconi, L. Lietti, R. Zennaro, P. Forzatti, Chem. Eng. Sci. 62 (2007) 5338–5343.
[38] C.G. Visconti, L. Lietti, E. Tronconi, P. Forzatti, R. Zennaro, S. Rossini, Catal. Today 154 (2010) 202–209.
[39] D. Vervloet, F. Kapteijn, J. Nijenhuis, J. Ruud van Ommen, Catal, Sci. Technol. 2 (2012) 1221–1233.
[40] D.E. Mears, J. Catal. 20 (1971) 127–131.
[41] R.R. Hudgins, Chem. Eng. Sci. 23 (1968) 93–94.
[42] S. LeViness, S.R. Deshmukh, L.A. Richard, H.J. Robota, Top. Catal. 57 (2014) 518–525.
[43] Istvan T. Horvath, Encyclopedia of catalysis, in: Mark E. Day (Ed.), Fischer-Tropsch Synthesis-Industrial, John Wiley & Sons, 2003, pp. 347–403.
[44] F.P. Incropera, D.P. De Witt (Eds.), Introduction to Heat Transfer, Wiley, 1996.
[45] R. Philippe, M. Lacroix, L. Dreibine, C. Pham-Huu, D. Edourard, S. Savin, F. Luck, D. Schweich, Catal. Today 147S (2009) S305–S312.
[46] M. Paturzo, M. Favaretto, M. Piazza, P. Forzatto, G. Groppi, L. Lietti, E. Tronconi, C. G. Visconti, Pat. WO/2014/102350.